

1 **Pore-scale hydrodynamics in a progressively bio-clogged**
2 **three-dimensional porous medium: 3D particle tracking**
3 **experiments and stochastic transport modeling**

4 **M. Carrel¹, V.L. Morales^{1,2}, M. Dentz³, N. Derlon^{1,4}, E. Morgenroth^{1,4}, M. Holzner¹**

5 ¹Institute of Environmental Engineering, ETH Zurich, Stefano Franscini-Platz 5, 8093 Zurich, Switzerland

6 ²Department of Civil and Environmental Engineering, University of California, Davis, California, USA

7 ³Spanish National Research Council (IDAEA-CSIC), c/Jordi Girona 18, 08034 Barcelona, Spain

8 ⁴EAWAG, Ueberlandstrasse 133, 8600 Dübendorf, Switzerland

9 **Key Points:**

- 10 • Experimental three-dimensional particle tracking of flow tracers allows Lagrangian
11 characterization of pore-scale hydrodynamics in a progressively bioclogged three-
12 dimensional porous medium.
- 13 • Biofilm growth induces formation of preferential flow paths and stagnation zones,
14 leading to an increase of anomalous transport.
- 15 • A Continuous Time Random Walk model based on a gamma distribution of the
16 pore-scale velocities captures transport dynamics.

Corresponding author: M. Holzner; V.L. Morales , holzner@ifu.baug.ethz.ch;
vermorales@ucdavis.edu

Abstract

Biofilms are ubiquitous bacterial communities that grow in various porous media including soils, trickling and sand filters. In these environments, they play a central role in services ranging from degradation of pollutants to water purification. Biofilms dynamically change the pore structure of the medium through selective clogging of pores, a process known as bioclogging. This affects how solutes are transported and spread through the porous matrix, but the temporal changes to transport behavior during bioclogging are not well understood. To address this uncertainty, we experimentally study the hydrodynamic changes of a transparent 3D porous medium as it experiences progressive bioclogging. Statistical analyses of the system's hydrodynamics at four time points of bioclogging (0, 24, 36 and 48 hrs in the exponential growth phase) reveals exponential increases in both average and variance of the flow velocity, as well as its correlation length. Measurements for spreading, as mean-square displacements, are found to be non-Fickian and more intensely superdiffusive with progressive bioclogging, indicating the formation of preferential flow pathways and stagnation zones. A gamma distribution describes well the Lagrangian velocity distributions and provides parameters that quantify changes to the flow, which evolves from a parallel pore arrangement under unclogged conditions, toward a more serial arrangement with increasing clogging. Exponentially evolving hydrodynamic metrics agree with an exponential bacterial growth phase, and are used to parameterize a correlated continuous time random walk model with a stochastic velocity relaxation. The model accurately reproduces transport observations and can be used to resolve transport behavior at intermediate time points within the exponential growth phase considered.

1 Introduction

Porous media flows are strongly affected by the ubiquitous structural heterogeneities of porous networks. Heterogeneity stems from wide distributions of pore sizes and length scales, which induce non-Gaussian or anomalous transport. This phenomenon is responsible for incomplete mixing or enhanced spreading, persistently spanning scales from the pore to the field [Berkowitz *et al.*, 2000; Gouze *et al.*, 2008; Le Borgne and Gouze, 2008; Dentz *et al.*, 2011; Le Borgne *et al.*, 2011a; Ederly *et al.*, 2014]. At the pore-scale, anomalous transport exhibits many different characteristics such as non-Gaussian velocity distributions [Bijeljic *et al.*, 2013; Matyka *et al.*, 2016], high temporal correlation of Lagrangian velocities forming a spatial Markov process [Le Borgne *et al.*, 2011b], intermittency of velocities along trajectories [de Anna *et al.*, 2013], and super-diffusive spreading [Kang *et al.*, 2014; Holzner *et al.*, 2015]. The intensity of the anomalous transport is related to the heterogeneity of the porous medium and has been investigated in media of different complexities, ranging from simple beadpacks to fractured sandstones and carbonates [Bijeljic *et al.*, 2013; Siena *et al.*, 2014; Meyer and Bijeljic, 2016; Morales *et al.*, 2017].

The distributions of pore sizes and length scales present in porous media can have a dynamic component driven by biological or physico-chemical processes, such as the development of bacterial biofilms [Stoodley *et al.*, 1994; Seymour *et al.*, 2004, 2007], mineral dissolution and precipitation [Daccord and Lenormand, 1987; Noiriél *et al.*, 2013; Menke *et al.*, 2015; Linga *et al.*, 2017], particle filtration in particle-laden flows [Bianchi *et al.*, 2018; Shen and Ni, 2017], or gas exchange in multiphase flows [Klump *et al.*, 2007; Datta *et al.*, 2013; Kazemifar *et al.*, 2016; Jiménez-Martínez *et al.*, 2016]. The resulting structural changes (e.g. porosity and permeability changes) influence the pore-scale hydrodynamics (e.g. pore-scale velocity distributions) and alter the system's anomalous transport intensity. In this work, we focus on the clogging of pores by bacterial biofilms. These sessile bacterial communities are of interest due to their ubiquitous presence in natural or industrial systems [Costerton *et al.*, 1999; Hall-Stoodley *et al.*, 2004]. Their relevance regarding porous media flows is in applications such as bioremediation [Bouwer and Zehnder, 1993], microbial enhanced oil recovery [Head *et al.*, 2003; Lazar *et al.*, 2007], and water treatment [Gujer and Boller, 1986; Leverenz *et al.*, 2009].

69 Biofilm development influences these different applications on a wide range of scales
70 [Ginn *et al.*, 2002; Battin *et al.*, 2007; Morgenroth and Milferstedt, 2009]. Therefore, differ-
71 ent experimental approaches have been used to study the impact of these systems. At the
72 field scale, the influence of biofilm development is generally monitored with geophysical
73 techniques [Atekwana and Atekwana, 2010] or with the use of tracer tests [Li *et al.*, 2010].
74 At the Darcy scale, several authors considered the influence of biofilm development on
75 macroscale properties (e.g. porosity, permeability etc.) using soil columns [Taylor and
76 Jaffé, 1990; Cunningham *et al.*, 1991; Vandevivere and Baveye, 1992; Lappan and Fogler,
77 1996; Thullner *et al.*, 2002]. At the pore scale, the use of optical visualization techniques
78 revealed how biofilm development altered the properties of two-dimensional pore networks
79 [Stoodley *et al.*, 1994; Dupin and McCarty, 1999; Kim and Fogler, 2000].

80 Recently, Coyte *et al.* [2017], showed that the growth of biofilm patches locally re-
81 duced the size of specific pores, which significantly affected the flow field. Biofilms were
82 experimentally [Seki *et al.*, 2006; Durham *et al.*, 2012; Nadell *et al.*, 2017] and numerically
83 [Pintelon *et al.*, 2009; Bottero *et al.*, 2013] observed to induce the formation of preferen-
84 tial flow pathways and stagnation zones in two-dimensional (2D) systems. Numerically,
85 Graf von der Schulenburg *et al.* [2009] combined lattice Boltzmann simulations with an
86 individual-based biofilm model to investigate the growth of biofilms in a 3D porous me-
87 dia. By comparing 2D and 3D results, the authors underlined the necessity of considering
88 three-dimensional systems, as the results in 2D or 3D differed substantially. For instance,
89 they showed that the variance of velocity distributions increased more slowly in 3D than
90 in 2D and the formation of preferential flow pathways was strongly delayed in 3D, war-
91 ranting experimental data to corroborate the findings. Ultimately, biofilms were shown to
92 cause an increase of non-Fickian transport dynamics [Seymour *et al.*, 2004, 2007; Knecht
93 *et al.*, 2011; Kone *et al.*, 2014].

94 The pioneering work by Seymour *et al.* [2004, 2007] provided direct access to pore-
95 scale velocity distributions in a progressively bioclogged porous medium. Additionally,
96 this work revealed a transition from Gaussian to non-Gaussian transport dynamics due to
97 biofilm development in a homogeneous beadpack. The authors used magnetic resonance
98 microscopy to quantify the evolution of propagators (i.e. displacement probability density
99 functions). The transition of the propagators was then modeled qualitatively for different
100 degrees of bioclogging using a conceptual continuous time random walk based on a power
101 law Lévy wait time and a Gaussian jump length distributions. However, this approach
102 does not honor the temporal correlation of the intermittent pore-scale flow, and thus does
103 not account for the spatial Markovian nature of porous media flows which was known to
104 be critical for accurate transport modeling [de Anna *et al.*, 2013]. The importance of this
105 temporal correlation is expected to increase with the heterogeneity induced by increasing
106 bioclogging [Le Borgne *et al.*, 2011b].

107 The goal of this study is to experimentally quantify the influence of biofilm growth
108 on pore-scale hydrodynamics to better understand and model flow and transport processes
109 in bioclogged systems. Lagrangian data from 3D Particle tracking velocimetry is used to
110 determine velocity distributions, mean square displacement and particle displacement dis-
111 tributions of flow particles at different bioclogging stages. Then, the hydrodynamic quan-
112 tities are statistically analyzed and their temporal evolution linked to expected trends of
113 biofilm growth. Lastly, these quantities are used to parameterize a correlated continuous
114 time random walk model that accurately captures transport observations and quantifies
115 flow transition from uniform to preferential.

2 Materials and Methods

2.1 Porous Media and Working Fluid

The porous medium used in this study consisted of Nafion pellets (NR50 1100 EW, Ion Power, Munich, Germany) of diameter $d_N \approx 2.5 \text{ mm}$, with similar physico-chemical properties to that of sand grains [Leis *et al.*, 2005; Downie *et al.*, 2012]. The refractive index of the Nafion pellets was matched with a working fluid made up of 11% w/v glucose aqueous solution. The optimal glucose concentration was defined using a protocol similar the one presented in Downie *et al.* [2012]. To ensure unlimited bacterial growth, the working solution was saturated with oxygen, nutrients (nitrogen, phosphorus) and electron acceptors (NaNO_3 , K_2HPO_4 and $\text{NaH}_2\text{PO}_4 \cdot 2(\text{H}_2\text{O})$) resulting in an influent solution with C:N:P molecular ratio of 1000:1:1. In order to optimize the refractive index matching, ca. 20 g of the Nafion pellets used were heated up in 250 mL of the glucose solution to 65 °C for one hour and cooled in a fresh solution overnight. This cycle was repeated three times.

2.2 Biofilm Growth and Hydrodynamic Conditions

The bacterial inoculum used in this study was isolated from the Chriesbach River (Dübendorf, Switzerland) [Desmond *et al.*, 2018]. Frozen bacterial stock contained in 2 mL Eppendorf tubes was added to 100 mL of the growth medium and incubated for 20-24 h at 30°C while stirring at 200 rpm until a midlogarithmic growth phase was reached ($\text{OD}_{600} 0.52 \pm 0.096$). Subsequently, 10 mL of the inoculum were added to 90 mL of fresh growth medium. This incubation procedure was repeated three times for the bacteria to adapt to the synthetic carbon source of the growth medium. An effective exponential growth rate of $0.097 \pm 0.012 \text{ 1/h}$ was measured by considering the OD_{600} (0.0505 ± 0.011) initially and once midlogarithmic phase was reached. The Nafion grains prepared following the protocol described above were added to the inoculum for the last incubation cycle to allow uniform initial bacterial attachment on the surface of the grains. A custom-built PMMA flow cell (inner dimensions: $38 \times 38 \times 16 \text{ mm}^3$) with point inlet and outlet openings at the bottom and top of the cell, respectively, was wet-packed with the inoculated Nafion grains.

A biofilm was allowed to grow in the fully water saturated packed flow cell for 48 h under a constant volumetric flow rate (10 mL/min, corresponding to an initial average residence time of ca. 40 s), which was set with a peristaltic pump (Ismatec, Glattbrugg, Switzerland). Note that the flux was kept constant. At this flow rate, the initial (prior to biofilm growth) Darcy velocity q was of 0.274 mm/s and the average interstitial pore velocity v_p was measured to be $\approx 1 \text{ mm/s}$, which yields an effective porosity $\phi = q/v_p$ of 0.27. This results in an initial Reynolds number of $Re = v_p d_N / \nu \approx 0.5$, where ν is the kinematic viscosity of the fluid. At the peak of observed biofilm growth, an observed threefold increase in v_p only raised Re to ≈ 1.5 , which is still within Darcy's law validity range ($Re \leq 10$). In this system, the Péclet number, defined as the ratio between advective, v_p , and diffusive transport rates, $D_{\text{H}_2\text{O}}/d_N$, was determined to be $Pe = \frac{v_p d_N}{D_{\text{H}_2\text{O}}} \approx 2500$, where $D_{\text{H}_2\text{O}}$ is the molecular diffusion coefficient of water.

2.3 3D-PTV Measurements

In this work, three-dimensional particle tracking velocimetry (3D-PTV) measurements were performed in a refractive index matched (RIM) [Budwig, 1994] porous medium to characterize the evolution of pore-scale hydrodynamics during biofilm growth. The open source 3D-PTV code employed here allows to quantitatively characterize different kind of flows by providing position, velocity and acceleration of tracer particles along trajectories ([Lüthi *et al.*, 2005; Hoyer *et al.*, 2005; Gülan *et al.*, 2012; Michalec *et al.*, 2015; Schmidt *et al.*, 2016]). 3D-PTV was first used to study flows in porous media by Moroni

165 and Cushman [2001]. Holzner et al. [2015] and Morales et al. [2017] used 3D-PTV to
166 study the intermittent nature of flows in heterogeneous 3D synthetic sandstone packings.
167 Shen and Ni [2017] used 3D-PTV to study the dynamics of filtration and clogging by par-
168 ticulate matter. Here, 3D-PTV was used to perform measurements over the course of the
169 biofilm growth, providing a quantitative description of the influence of biofilm growth on
170 flow and transport.

171 3D-PTV measurements were performed at time points $T = 0, 24, 36$ and 48 h of
172 biofilm culturing [Carrel et al., 2018a]. To perform the 3D-PTV measurements, a syringe
173 connected to the flow cell was mounted on a syringe pump (Lambda Vit-Fit, Lambda,
174 Baar, Switzerland). Fluorescent tracer particles (Red Polyethylene Microspheres, Cospheric,
175 Santa Barbara, CA USA) of diameter $d_P \approx 70 \mu\text{m}$, density $\rho_P = 0.995 \text{ g/cm}^3$, and neu-
176 tral buoyancy (Stokes number $Stk \ll 1$), were seeded to the flow and tracked in time and
177 3D space with 3D-PTV. The Péclet number of the tracers can be considered to be infinite
178 due to the size of the particles and their corresponding negligible diffusivity. The tracer
179 particle concentration used was of 0.02 g/L (volume fraction concentration $\approx 0.002 \%$), to
180 which 0.2 ppm of surfactant (Tween, Cospheric, Santa Barbara, USA) was added to pre-
181 vent particle agglomeration during the 3D-PTV measurements. We note that the tracer
182 particles are too large to enter the sub-micrometer sized inner biofilm channels [Stood-
183 ley et al., 1994; Carrel et al., 2017] and that the particle to Nafion pellet diameter ratio
184 d_N/d_P is of ca. 35. Thus, the effective porosity reduction of the porous medium due to
185 interception of the tracer particles can be considered to be insignificant [Sakthivadivel and
186 Einstein, 1970; Yao et al., 1971]. Additionally, due to the extremely low volume fraction
187 concentration, particle-particle interactions can be neglected.

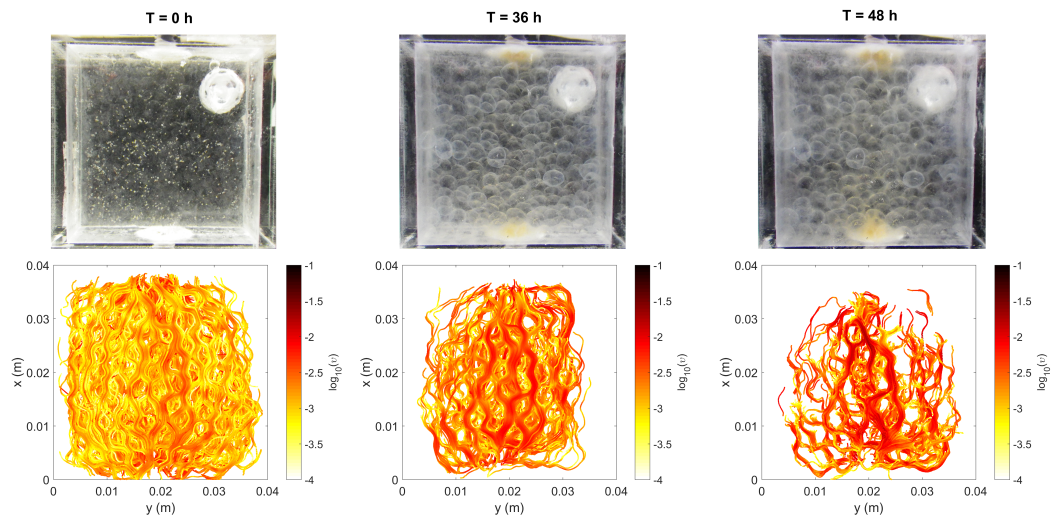
188 Once the flow fluid was seeded, the particles were then illuminated with a 100 W
189 pulsed Nd-YLF laser (Darwin Duo, Quantronix, Hamden, USA). Images were acquired
190 with a Photron Fastcam SA5 at 50 Hz with 1 Mega pixel resolution. An image splitter
191 was used to mimic a four camera system that permits stereoscopic viewing of the sam-
192 ple. A redundant 4 views system allows highly accurate particle recognition and track-
193 ing [Maas et al., 1993; Malik et al., 1993; Lüthi et al., 2005]. For particle recognition, a
194 pre-processing step consisting of a running image subtraction with a lag of 50 images
195 and a high pass filter were applied to improve the signal to noise ratio of individual video
196 frames. Subsequent rejoining of fragmented trajectories was achieved with a 6D position-
197 velocity search that reconnects trajectory fragments when their velocity and acceleration
198 vectors match with a small tolerance [Xu, 2008]. A Savitzky-Golay filter was then imple-
199 mented in order to smooth trajectories [Saha et al., 2014]. The final sub-pixel accuracy
200 of the particle positions along trajectories was estimated to be of about $50 \mu\text{m}$ [Holzner
201 et al., 2015]. Short or immobile trajectories with total displacement shorter than 1 mm or
202 0.5 s , respectively, were discarded from the analysis. This yielded more than $O(10^3)$ high
203 quality trajectories to analyze in the bioclogged porous medium for each time point (4465,
204 3604, 1953 and 2660 for the time points $T = 0, 24, 36$ and 48 h respectively). The veloc-
205 ity and Lagrangian acceleration was calculated using centered finite differences of position
206 and velocity, respectively, along particle trajectories. Given that pressure transducers were
207 not available in the experiment we estimated permeability indirectly as follows. We calcu-
208 lated the Laplacian of velocity after interpolating the velocity data onto an Eulerian grid
209 with a spacing of 0.2 mm . This allowed estimating the pressure difference Δp between in-
210 and outlet by integrating the local pressure gradient $\nabla p = -\rho(Dv_p/Dt - v\nabla^2 v_p)$ along
211 streamlines, where ρ is the density fo the fluid and D/Dt denotes the material derivative.
212 The permeability was then estimated from Darcy’s law as $k = \phi v_p \nu L_x / \Delta p$, where L_x is
213 the length of flow cell. In the course of the experiment, the growing biofilm increasingly
214 attenuated the signal emitted by the tracer particles. The experiment was stopped after 48
215 h of biofilm growth, as tracer particles could be detected well only up to 50% of the flow
216 cell depth. In order to compensate for the increasing light attenuation and to image parti-
217 cle tracers over the whole flow cell depth, images were acquired from both front and back
218 sides of the flow cell. Over the course of the experiment, the average trajectory length re-

219 maintained relatively constant at around 25 % of the total flow cell length (26, 28, 33 and 22
 220 % for the time points $T = 0, 24, 36$ and 48 h respectively). With the growth of biofilm the
 221 transparency of the media decreased which led to a decrease in the number of reconstructed
 222 particle tracks. The RIM quality was not affected significantly. We assessed the RIM by
 223 placing a pattern of straight lines behind the test sample and by calculating the scaled root
 224 mean square error of linear fit regressions. Before biofilm growth, RIM was excellent and
 225 comparable to results in Downie et al. (2012). During bioclogging, the RIM quality de-
 226 creased only slightly, i.e. from about $50 \mu\text{m}$ at $T=0$ hrs to about $70 \mu\text{m}$ at $T=36$ hrs. This
 227 decrease is not substantial and on the same order of the accuracy of the 3D determination
 228 of tracer particle locations. It therefore did not significantly affect the particle tracking. Fi-
 229 nally, to account for entry effects at a point inlet, data at the first advective time scale τ_A
 230 of each trajectory was discarded. Here, $\tau_A = \lambda_i / \langle v \rangle$, where λ_i is the length scale of the
 231 system and $\langle v \rangle$ is the average velocity (see Table 1).

3 Results

3.1 Experimental pore-scale characterization of the progressive bioclogging

234 Figure 1 top row shows photographs of the flow cell during biofilm culturing (top)
 235 after 0, 36 and 48 h. The photographs illustrate how the biofilm progressively develops in
 236 the flow cell. Note that the transparency of the flow cell decreases with biofilm growth.
 237 Figure 1 bottom row shows equivalent projections of 3D-trajectories (more than 10^6 data
 238 points for each case) color-coded with the logarithm of the norm of the velocity vector.



239 **Figure 1.** Photographs illustrating progressive changes in the porous media with increasing bioclogging of
 240 the flow cell (top) and particle trajectories obtained by 3D-PTV (bottom) for the time points $T = 0, 36$ and 48
 241 h. The bright spot in the upper right corner of the photographs is a reflection by a teflon-coated plastic screw
 242 that is used to close the opening of the flow cell. The trajectories are color-coded with the logarithm of the
 243 norm of the velocity vector.

244 The trajectories display intermittent Lagrangian velocities inherent to fluid flows in
 245 porous media [de Anna et al., 2013; Kang et al., 2014; Holzner et al., 2015; Morales et al.,
 246 2017], accelerating at pore throats and decelerating at pore bodies [Holzner et al., 2015].
 247 The flow cell is operated with a constant flow rate, so that biofilm growth in the system
 248 increases the average longitudinal velocity, as illustrated by the increasingly darker color-

249 coding of the trajectories. Note that the photographs and the trajectories of Figure 1 are
 250 only qualitatively aligned for visual comparison. As larger amounts of biofilm form in the
 251 flow cell, tracer particles are confined to fewer channels in the domain. Mass conservation
 252 corroborates such channel formation as it is observed in the ca. 3 fold increase in longi-
 253 tudinal velocity (see table 1). Consequently, regions not sampled by the particles can be
 254 considered to be stagnation zones occupied by biofilm or newly formed stagnant zones,
 255 and thus do not contribute to carrying the flow. With increasing bioclogging, more of
 256 these stagnation zones appear. It is visible qualitatively that these stagnant zones in Fig-
 257 ure 1 (trajectories for $T = 48$ h) correlate with the opaque bioclogged regions in Figure 1
 258 (photograph for $T = 48$ h).

259 3.2 Lagrangian velocity probability density functions

In order to quantitatively investigate the influence of progressive bioclogging on
 porous media flow, we first consider probability density functions (PDFs) of isochronic
 Lagrangian velocities (t-Lagrangian) along the trajectories [Moroni and Cushman, 2001;
 Moroni et al., 2007; Holzner et al., 2015; Morales et al., 2017]. Under ergodic conditions
 and for incompressible flow, the t-Lagrangian velocity PDF is equivalent to the Eulerian
 velocity PDF [Dentz et al., 2016]. The PDFs of t-Lagrangian velocities $P_t(v)$ are obtained
 by

$$P_t(v) = \frac{1}{N_p} \sum_{i=1}^{N_p} \frac{1}{T_i} \int_0^{T_i} dt \frac{\mathbb{I}[v \leq v(t; \mathbf{a}_i) < v + \Delta v]}{\Delta v}, \quad (1)$$

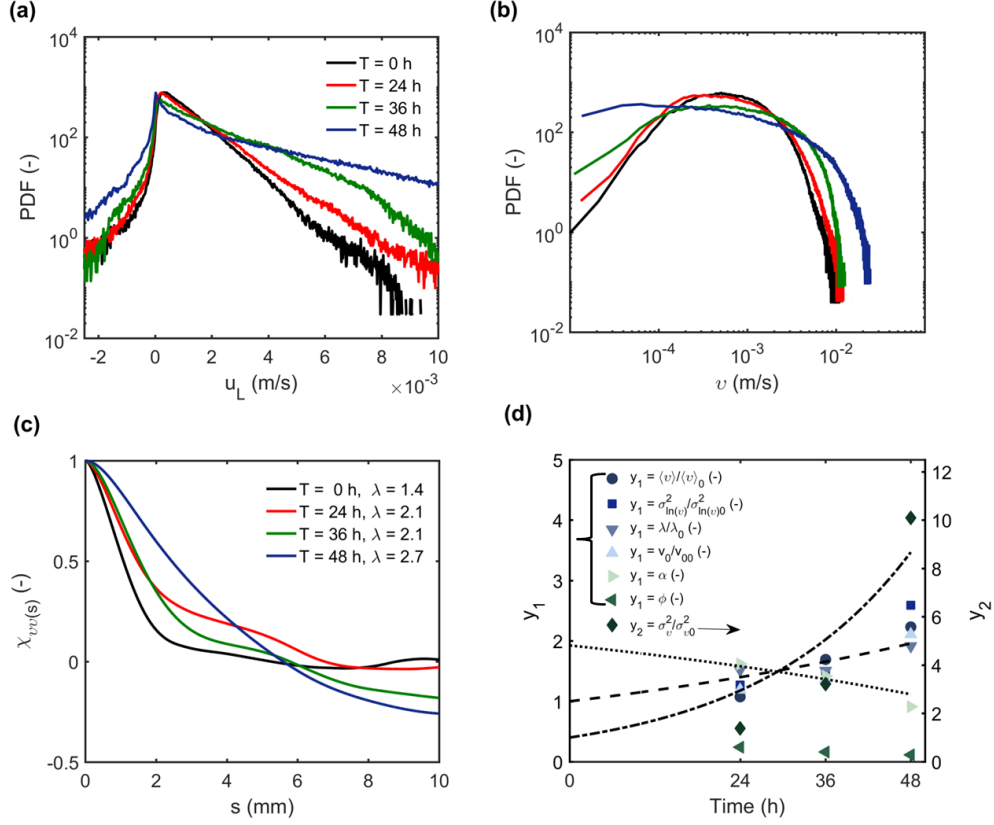
260 where N_p is the number of trajectories, \mathbf{a}_i is the initial point of the i th trajectory, T_i is the
 261 duration. $v(t; \mathbf{a}_i)$ denotes the longitudinal or transverse components of the particle veloc-
 262 ity, $\mathbf{v}(t; \mathbf{a}_i)$ is its magnitude, and Δv is the sampling interval.

263 The PDFs of the t-Lagrangian velocities in longitudinal and transverse directions as
 264 well as for the velocity magnitude for the four time points during biofilm growth are illus-
 265 trated in Figure 2 (a) and (b). As listed in Table 1, upon biofilm growth and subsequent
 266 effective porosity reduction, the average velocity in the system increases due to fluid mass
 267 conservation.

277 As Figure 2 (a) and (b) shows, the PDFs of the longitudinal velocity component and
 278 of the velocity magnitude exhibit a substantial increase in variance and tailing heftiness.
 279 The variance increase of the velocity magnitude (see σ_v^2 in Table 1) reflects the forma-
 280 tion of preferential flow paths of high velocities, as the variance σ_v^2 is dominated by the
 281 contribution of velocities much higher than the mean $\langle v \rangle$. Therefore, we also report the
 282 variance of the natural logarithm of the velocity (see $\sigma_{\ln(v)}^2$ in Table 1), which increase
 283 nearly three fold and give insight on the increase of width toward low velocities. Higher
 284 probability of finding low velocities is a result of the formation of zones of almost stag-
 285 nant flow.

291 3.3 Velocity auto-correlation functions

292 The spatial auto-correlation length of Lagrangian velocities has previously been
 293 identified to reflect the spatial Markovian nature of flows in porous media [Le Borgne
 294 et al., 2008]. We therefore determine the Lagrangian velocity magnitude auto-correlations
 295 during progressive bioclogging. An increase in spatial correlation is indicative of persis-
 296 tent fast velocities along trajectories, and suggests the formation of preferential flow paths.



268 **Figure 2.** Probability density functions of the t-Lagrangian (a) longitudinal velocity component and (b)
 269 magnitude obtained at different time points. (c) shows the auto-correlation function of the velocity magnitude,
 270 indicating the corresponding correlation lengths (characteristic length of the system) in the legend. (d) illus-
 271 trates the temporal evolution of the average velocity $\langle v \rangle$, the variance of the natural logarithm of the velocity
 272 $\sigma_{\ln(v)}^2$, the correlation length λ , and of the characteristic velocity v_0 , as normalized by their value at the time
 273 point $T = 0$ h. The dashed line shows an exponential fit with growth rate $c = 0.015 \text{ h}^{-1}$. The evolution of α
 274 (with dotted line representing the corresponding exponential fit with $c_\alpha = 0.012 \text{ h}^{-1}$) and of the effective
 275 porosity ϕ are illustrated on the same y-axis. The evolution of the normalized velocity variance σ_v^2/σ_{v0}^2
 276 is shown on the secondary y-axis (with the dashed-dotted line showing the corresponding fit, $c_{\sigma_v^2} = 0.045 \text{ h}^{-1}$).

297 The auto-correlation functions of the s-Lagrangian velocity magnitude $v_s(s; \mathbf{a})$ [Dentz
 298 *et al.*, 2016] sampled equidistantly along a trajectory are defined as:

$$\chi_{vv}(\Delta s) = \frac{\sum_{i=1}^{N_p} R_{vv}(\Delta s; \mathbf{a}_i)}{\sum_{i=1}^{N_p} \sigma_{vv}^2(\mathbf{a}_i)}, \quad (2)$$

where the velocity covariance along a single trajectory is defined by

$$R_{vv}(\Delta s; \mathbf{a}_i) = \frac{1}{L_i} \int_0^{L_i} ds [v_s(s + \Delta s; \mathbf{a}_i) - \langle v_s(s) \rangle] [v_s(s; \mathbf{a}_i) - \langle v_s(s + \Delta s) \rangle]. \quad (3)$$

286 **Table 1.** Average velocity magnitude $\langle v \rangle$, velocity magnitude variance σ_v^2 , correlation length scale λ of the
 287 t-Lagrangian velocity magnitudes, scale parameter v_0 expressing a characteristic velocity, shape parameter α
 288 informing the system connectivity, porosity and permeability for all time points $T = 0, 24, 36$ and 48 h. c_i is
 289 the exponential coefficient and R_i^2 is the coefficient of determination for the exponential change in time of the
 290 listed hydrodynamic parameters.

	T = 0 (h)	T = 24 (h)	T = 36 (h)	T = 48 (h)	c_i (1/h)	R_i^2
$\langle v \rangle$ (mm/s)	1.3	1.4	2.2	2.9	0.015	0.85
σ_v^2 (m ² /s ²)	9.82E-07	1.35E-06	3.16E-06	9.91E-06	0.045	0.86
$\sigma_{ln(v)}^2$ (-)	0.651	0.825	0.975	1.686	0.017	0.81
λ (mm)	1.38	2.1	2.1	2.7	0.013	0.92
v_0 (-)	0.518	0.616	0.705	1.093	0.013	0.79
α (-)	1.929	1.619	1.418	0.914	0.012	0.95
ϕ (-)	0.27	0.24	0.19	0.12	0.012	0.89
$\phi/\phi(t=0)$ (-)	1	0.89	0.70	0.44	0.012	0.89
k (cm/s)	1.74	1.40	1.03	0.50	0.014	0.92
$k/k(t=0)$ (-)	1	0.80	0.60	0.29	0.014	0.92
Δs (mm)	0.0138	0.021	0.021	0.027	-	-

299 where $v_s(s; \mathbf{a})$ is the velocity magnitude along the trajectory which starts at \mathbf{a} , measured
 300 in distance s traveled along the trajectory, and L is the length of the trajectory. The veloc-
 301 ity variance along the trajectory is given by $\sigma_{vv}^2(\mathbf{a}) = R_{vv}(0; \mathbf{a})$. Finally, the correlation
 302 length, λ , is obtained by integration of χ_{vv} .

303 Figure 2 (c) shows the auto-correlation functions of the s-Lagrangian velocity mag-
 304 nitudes obtained from the 3D-PTV measurements for all time points and the correspond-
 305 ing correlation lengths obtained by integration for the different data sets. As these results
 306 show (see Figure 2 (c) and Table 1), the correlation length measured along trajectories in-
 307 creases from approximately $\lambda \approx d_N/2$ to $\lambda \approx d_N$, where $d_N \approx 2.5$ mm is the average
 308 nanion pellet diameter. This implies that with increasing growth of biofilm, the pore struc-
 309 ture of the medium becomes more spatially correlated.

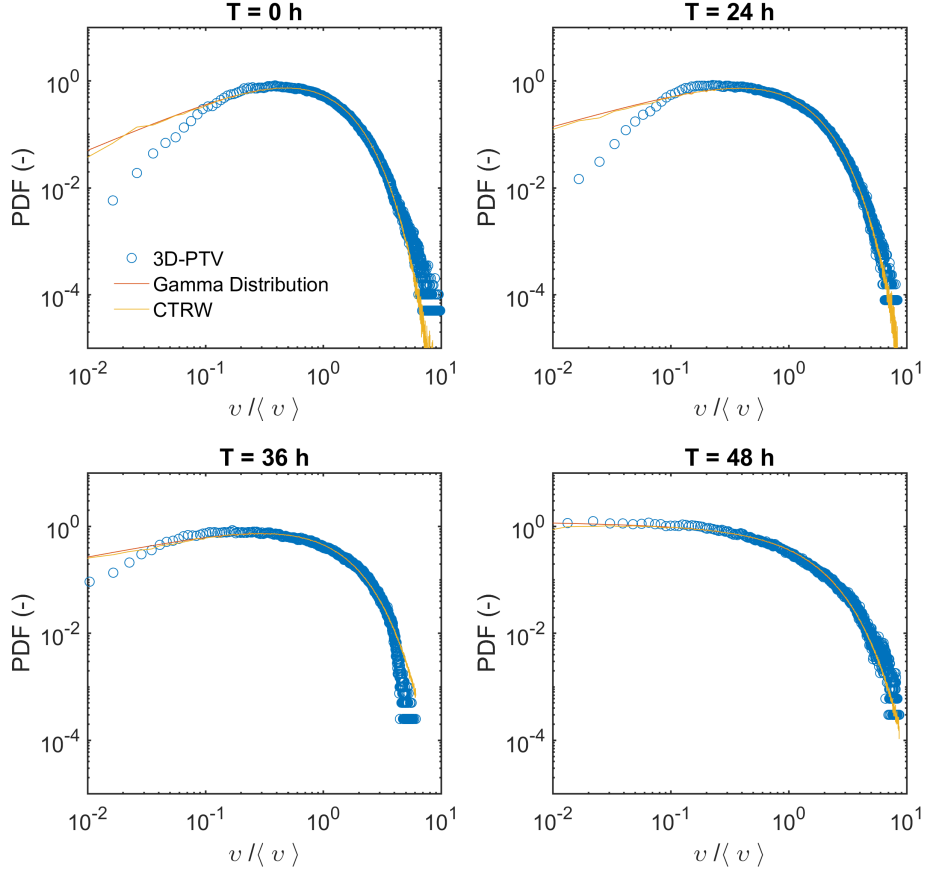
310 3.4 Approximation of the velocity magnitude with a gamma distribution

Hereinafter, we consider the t-Lagrangian velocity magnitude for all time points pre-
 sented in Figure 2 (b). We find that the PDF of the t-Lagrangian velocity magnitude can
 be approximated by the following gamma distribution

$$\mathcal{P}(v_t) = \frac{v^{\alpha-1}}{v_0^\alpha \Gamma(\alpha)} e^{-\frac{v}{v_0}} \quad (4)$$

311 This function captures the increasing heterogeneity in the system upon biofilm growth in
 312 the evolving function parameters α , the exponent, (probability weight at low velocities,
 313 refer to Table 1 for values for each time point) and v_0 , the scaling parameter (a character-
 314 istic velocity reflecting the increase in the average velocity). The reader is referred to Table
 315 1 for parameter values at each time point).

319 Figure 3 shows the 3D-PTV velocity magnitudes for all time points and the corre-
 320 sponding gamma distributions with shape and scale parameters estimated by maximum
 321 likelihood estimation (MLE). As listed in Table 1, the exponent α which represents the
 322 connectivity of the pore network [Holzner et al., 2015] decreases substantially. Holzner
 323 et al. [2015] presented a theoretical consideration that the maximal and minimal values



316 **Figure 3.** Probability density functions of the velocity magnitudes obtained with 3D-PTV, the correspond-
 317 ing MLE gamma distributions and the PDFs of the velocity obtained from the CTRW model for all time
 318 points.

324 of α were 2 and -2 for completely serial or parallel pore arrangements, respectively. The
 325 decrease of α observed in Table 1 from 1.929 to 0.914 therefore suggests that the struc-
 326 ture of the pore network evolves from a predominantly parallel pore arrangement towards
 327 a more serial pore arrangement. The characteristic velocity v_0 increases substantially, sim-
 328 ilar to the average velocity increase upon biofilm growth and the corresponding reduc-
 329 tion of the void space. This finding is in agreement with other studies at the column and
 330 catchment scale, which have also observed gamma distributed velocity and residence times
 331 [Wen and Li, 2017; McGuire et al., 2005].

332 3.5 Temporal evolution of the hydrodynamic quantities

333 The temporal evolution of various hydrodynamic characteristics of the system is pre-
 334 sented in Figure 2d. We expect that the measured changes of these quantities mirror the
 335 exponential increase of biomass in the system over time. The growth of biomass equates
 336 to porosity reduction. This structural change, combined with mass conservation of a sys-
 337 tem at constant flux, explains the exponential increase in average pore velocity given that
 338 $\langle v \rangle = q/\phi$ where q is the fixed Darcy flux and ϕ is the effective porosity. A similar ex-
 339ponential evolution in the velocity variance, correlation length scale, and gamma function

parameters (v_0 and α) is observed and justified by the same logic. Table 1 summarizes the exponential coefficients associated with each hydrodynamic quantity following the expression $X(t) = X_0 e^{c_i t}$, where X_0 is the value of the considered quantity at the time point $T = 0$ h and c_i is the corresponding exponential constant. The structural changes that lead to increased flow heterogeneity also affect the average flow properties through a gradual reduction of permeability, which, however, decreases more sharply than porosity (see Table 1 and compare relative values of $k/k(t=0)$ and $\phi/\phi(t = 0)$). This indicates a gradual reduction of pore connectivity due to bioclogging (Carrel *et al.* [2018b]).

3.6 Correlated continuous time random walk

To investigate the influence of the formation of preferential flow paths and stagnation zones on transport processes, we employ a correlated continuous-time random walk (CTRW) model that simulates pore-scale particle motion [Le Borgne *et al.*, 2011b; de Anna *et al.*, 2013; Holzner *et al.*, 2015]. CTRW models provide an efficient modeling approach for transport in velocity fields that vary over a characteristic length scale [Dentz *et al.*, 2016]. As discussed in the previous section, s-Lagrangian particle velocities vary over a correlation scale λ , or in other words particle velocities persist over the characteristic length scale λ , which changes according to the growth of the biofilm. We assume that the evolution of λ is much slower than the typical particle transport scales. Thus, particle motion is modeled by the following recursion relation.

$$s_{n+1} = s_n + \Delta s, \quad t_{n+1} = t_n + \frac{\Delta s}{v_n} \quad (5)$$

Here, $v_n = v_s(s_n)$ and Δs a space increment. The velocity series $\{v_n\}$ is modeled by a stochastic relaxation process [Dentz *et al.*, 2016] to account for the correlation of velocities inherent to the spatial Markovian nature of flows in porous media [Le Borgne *et al.*, 2008, 2011b; de Anna *et al.*, 2013]. The steady state PDF $P_s(v)$ of the spatial Markov chain $\{v_n\}$ is obtained from $P_t(v)$ through flux-weighting as [Dentz *et al.*, 2016]

$$P_s(v) = \frac{v P_t(v)}{\langle v_t \rangle}. \quad (6)$$

Particles can maintain or change their velocity at turning points after n steps according to a Bernoulli process with persistence probability $p = \exp[-\Delta s'/(2\lambda_T')]$ or randomly sample from the velocity distribution by $P_s(v)$ according to $1 - p$. The single quotation mark indicates the normalization of the spatial increments Δs (see Table 1) and of λ_T by the reference length scale λ_T (for $T = 0, 24, 36$ and 48). The persistence of the velocity p over the spatial increments is based on an exponential decorrelation over twice the computed correlation length in order to account for incomplete mixing at pore throats. In the following, particle transport is simulated by Equation 5 for the different time points and the corresponding correlation lengths λ_T . The PDFs of the t-Lagrangian velocity magnitude obtained from the correlated CTRW in figure 3 show good agreement with the experimental data and with the fitted gamma distributions.

3.7 Displacement statistics

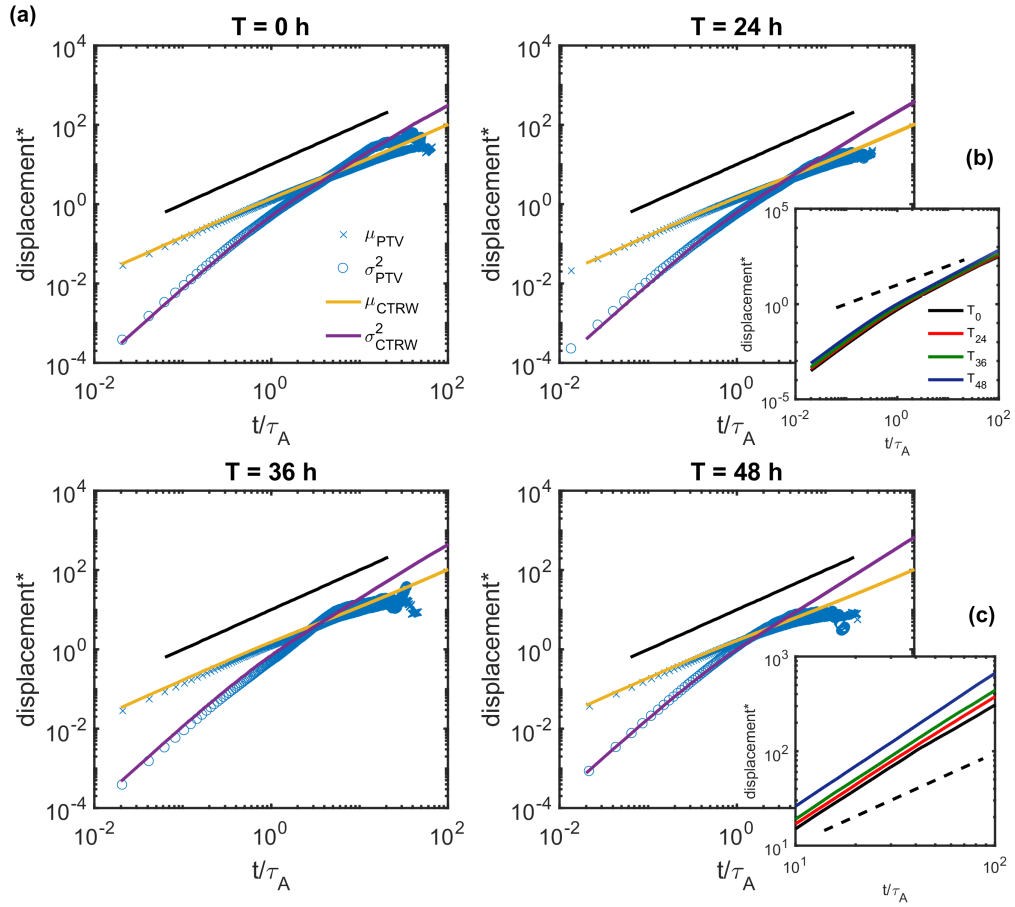
The displacement $s(t)$ at a given time t is given in terms of the CTRW model by $s(t) = s_{n_t}$, where $n_t = \max(n | t_n \leq t)$. We study the mean and centered mean squared displacements

$$m(t) = \langle s(t) \rangle, \quad \sigma_s^2(t) = \langle s(t)^2 \rangle - m(t)^2, \quad (7)$$

obtained from the 3D-PTV data, and interpret them in the light of the correlated CTRW model discussed above. This gives some insight into the heterogeneity of the porous medium

373
374

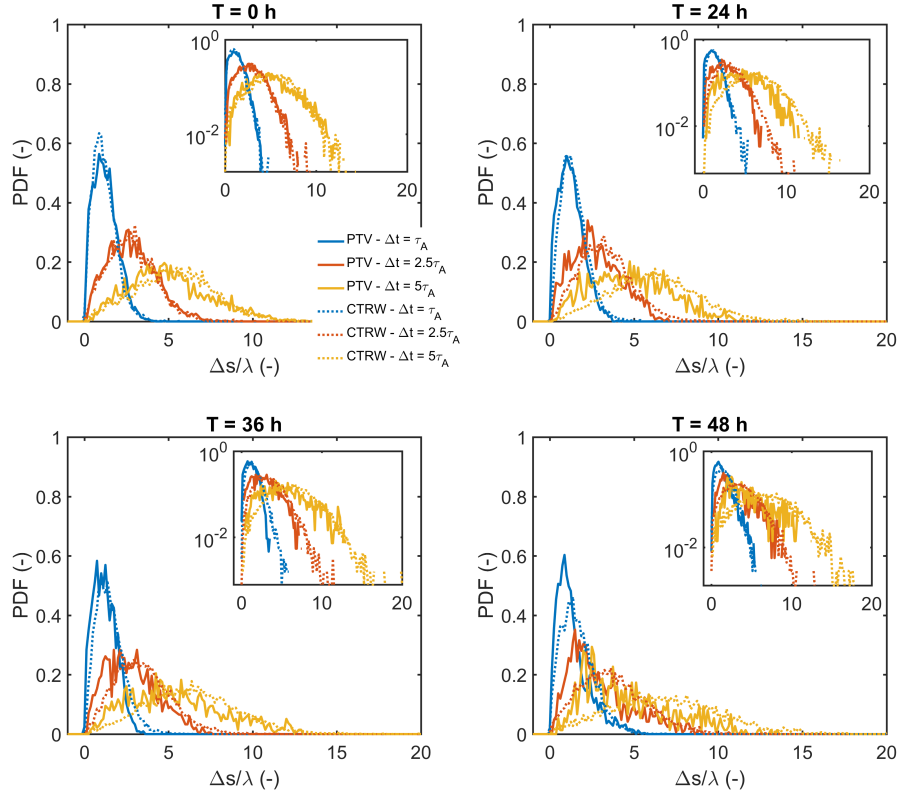
and the role of biofilm growth for particle dispersion. The angular brackets denote the average over all particles.



375 **Figure 4.** (a) Experimental (3D-PTV) and numerical (CTRW) mean m and mean-squared displacements
 376 σ^2 obtained for all time points. The spatial moments presented here are dimensionless, as they are rescaled
 377 by the corresponding length scales (λ or λ^2). The time is rescaled by the advective time scale τ_A . (b) CTRW
 378 mean-squared displacements for all the different time points. (c) Magnification of (b) illustrating a moderate
 379 increase in superdiffusive behavior with increasing biofilm growth. The continuous lines in (a) or (b) and (c),
 380 respectively, indicate Fickian scaling ($\sigma_s^2(t) \propto t$).

381 Figure 4 (a) shows the evolution of the first and second centered displacement moments of the 3D-PTV experimental data and of the CTRW for all time points. The mean
 382 displacement is consistently well captured by the CTRW model. All experimental mean-squared displacements (MSDs) $\sigma_s^2(t)$ show a transition from a ballistic regime ($\sigma_s^2(t) \propto t^2$)
 383 to a superdiffusive regime with a temporal scaling greater than the expected asymptotic Fickian regime ($\sigma_s^2(t) \approx t^{1.5}$). Here, a transition between ballistic and superdiffusive
 384 regimes occurs at about one advective time scale. Both regimes as well as the transition are captured by the CTRW model. Note the discontinuity and interruption of the experi-
 385 mental data after 5 to 10 advective time scales τ_A due to the finite size of the experimen-
 386 tal field of view and of the trajectory lengths. In Figure 4, the insets (b) and (c) show the evolution of the mean-squared displacements obtained from the CTRW (b) and a magni-
 387 fication of the superdiffusive regime (c). The vertical shift of the MSDs with progressive
 388
 389
 390
 391
 392

393 bioclogging is due to the increasing variance of the velocity magnitude (see Figure 4 (b)
 394 or refer to Table 1). The exponent of these MSDs slightly increases with bioclogging (see
 395 Figure 4 (c)), suggesting that the formation of preferential flow pathways and stagnation
 396 zones upon biofilm growth leads to an increase of anomalous transport.



397 **Figure 5.** Conditional displacement probability density functions for the 3D-PTV and the CTRW data for
 398 all the different time points. The semi-logarithmic insets shows that the propagators never reach a fickian
 399 regime where they would follow a Gaussian distribution.

400 3.8 Conditional displacement PDFs

401 In order to further investigate how well the presented model captures transport processes,
 402 we consider the conditional displacement PDFs along particle trajectories (also
 403 known as propagators), defined as $P(s + \Delta s | s, \Delta t)$ from s to s' for a given time lag Δt . Figure
 404 5 illustrates the 3D-PTV and the CTRW propagators obtained for all time points in the
 405 porous medium considered. These propagators were computed for normalized time lags
 406 corresponding to 1, 2.5 and 5 advective time scales. The semi-log propagators in the inset
 407 show that the transport regime remains superdiffusive for all the time lags considered for
 408 all time points, and that a Gaussian displacement distribution is not reached for the time
 409 lags defined. Interestingly, the skewness (i.e., third spatial moment) of the propagators
 410 increases with progressive bioclogging, as the heterogeneity of the flow and anomalous
 411 transport in the system increase as well. The CTRW model performs very well for the
 412 clean porous medium ($T = 0$ h). For later time points, however, the increased skewness of
 413 the propagators is less well captured by the model.

4 Discussion

In this study, 3D-PTV measurements were performed during biofilm growth in a porous medium to quantify how biofilm growth affects pore-scale hydrodynamics and the resulting transport behavior. The growth of biofilm induced an increase of anomalous transport in the considered system. A correlated continuous time random walk model parameterized by the gamma distributed pore-scale velocity magnitudes accurately captures the mean and mean-squared displacement changes, and qualitatively reproduces displacement probability density functions with lesser skewness.

The average velocity and further hydrodynamic quantities follow an exponential evolution with biofilm growth, which for all quantities except the variance σ_v^2 can be described by an exponential time scale of approximately 0.015 h^{-1} . We conjecture that this behavior is due to the exponential growth of the bacteria in the considered system. During incubation, the effective growth coefficient of the bacteria was measured to be of approximately 0.09, which is about one order of magnitude larger than the exponential coefficients observed for the hydrodynamic quantities. However, this difference could be attributed to the fundamental differences in growth kinetics of planktonic and sessile bacteria. Additionally, detachment of bacteria might also have induced a lower exponential growth coefficient. It is logical to expect that the effective porosity, and consequently the average velocity, will increase at a rate that is imposed by the increase of biomass in the porous medium. Similar obtained rates for geometrical parameters of the medium (correlation length λ and connectivity parameter α) are less trivial to justify physically. We nevertheless propose a similar logic to explain their temporal evolution, given that these characteristics depend on average pore-scale geometry (i.e. length scale and pore arrangement) and therefore are proportional to the amount of biomass produced. Differently, the rate of change in velocity variance is found to be about three times higher with biomass growth. The large increase in variance can be justified by the patchy growth of biomass throughout the porespace. This induces blockage to flow in certain pores (which governs transitions in slow velocities) and develops preferential paths in others (which governs the high velocities). The inclusion of much slower and much faster observed velocities is captured in the increase of distribution variance, which is a quantity independent of mean velocity.

In the literature, the flow velocity distribution is often discussed separately for two distinct regimes, i.e. the slow flow zones associated with stagnant zones and the fast velocities or preferential pathways carrying most of the fluid transport. The question on a mechanistic understanding between pore-scale organization of the media and the resulting flow velocity distribution for both regimes has been addressed since many years and still remains a challenge. *Saffman* [1959] used Poiseuille's law as an approximation of the flow in individual pores to relate velocity and pore diameter, which gives a map of pore diameter to pore velocity. This approach was used in *Holzner et al.* [2015] to obtain the distribution of pore velocities according to a Gamma function, which implies a power law behavior for small velocities and exponential decay of fast velocities that is consistent with their experiments and other previous studies in heterogeneous media (see references in *Holzner et al.* [2015]). *de Anna et al.* [2017] recently succeeded in deriving a direct relationship between the pore size distribution and the velocity distribution for the slow velocities. Namely, they showed that the velocity distribution follows a power law where the power is half of the power given by the pore size distribution. The fast velocities are given by the conductive backbone and its distribution varies from medium to medium (e.g. *Matyka et al.* [2016]). *Alim et al.* [2017] presented an analytical model, where the local correlations between adjacent pores, which determine the distribution of flows propagated from one pore downstream, predict the high tail of the flow distribution. They showed that, starting from a highly ordered bead pack and increasing the level of disorder, the fast velocities transitioned from Gaussian towards exponential distribution. In summary, at the pore scale, the distribution of pore sizes controls the low tail [*de Anna et al.*, 2017]

467 and correlations of fluxes between adjacent pores control the high tail of the velocity dis-
468 tribution. In our work, the growing biofilm reduces pore spaces in slow velocity zones
469 which will increase the probability of small radii and consequently the low tail of the ve-
470 locity PDF. Given that low velocity zones become less conductive, more and more flux is
471 carried in faster velocity regions, which presumably increases correlations between sub-
472 sequent pores along preferential pathways. This non-local effect seems thus at the root of
473 the intensification of the high tail of the velocity PDF we observed here in the bioclogged
474 media.

475 As the pore-space is reduced upon biofilm growth, the velocities in narrowing pores
476 increase on average. However, we also observe an increase of the probability of low veloc-
477 ities. This increase can be attributed to the narrowing pore size as according to Poiseuille's
478 law for flow through a pipe (an idealization of a single pore throat). In such a case, the
479 maximum velocity is proportional to the pore diameter squared for a constant pressure
480 gradient. The increase of probability of low velocities due to the narrowing pore size sug-
481 gests the formation of almost stagnant zones, which marginally contribute to the total flow.
482 Note however that locally, neither the mass flux nor the pressure gradient are fixed and
483 therefore, the structural changes caused by the biofilm growth induce an increase of the
484 variance of the velocity distributions, whose PDFs become increasingly non-Gaussian.
485 *Bijeljic et al.* [2013]; *Datta et al.* [2013]; *Siena et al.* [2014]; *Matyka et al.* [2016]; *Meyer*
486 *and Bijeljic* [2016] made similar observations for porous media with different pore net-
487 work characteristics (effective porosity, tortuosity, pore size distribution, connectivity etc.),
488 showing that the non-Gaussianity of the velocity PDFs was caused by the structural het-
489 erogeneity of the porous medium considered or by different degrees of saturation for par-
490 tially saturated porous media. Additionally, several authors have also reported increas-
491 ing exponents of the superdiffusive regime of the MSDs for porous media or fracture
492 networks exhibiting increasing degrees of heterogeneity [*Meyer and Bijeljic*, 2016; *Kang*
493 *et al.*, 2017].

494 Note that porosity-permeability relationships, which have been frequently studied in
495 the literature [*Taylor and Jaffé*, 1990; *Cunningham et al.*, 1991; *Vandevivere and Baveye*,
496 1992; *Lappan and Fogler*, 1996; *Thullner et al.*, 2002], refer to the relation of the aver-
497 age flow velocity to the average pore volume. As shown above, the observed (anomalous)
498 transport behavior can be attributed to the low end of the velocity PDF and cannot be un-
499 derstood by considering the mean velocity alone. Thus, in order to predict the influence of
500 biofilm growth on flow and transport behavior it would be desirable to determine the re-
501 lation between flow velocity and pore size distribution, and between pore size distribution
502 and biofilm growth. Velocity models based on Poiseuille's law [*Saffman*, 1959; *Holzner*
503 *et al.*, 2015; *de Anna et al.*, 2017; *Dentz et al.*, 2018] relate the behavior of the velocity
504 PDF at low velocities to the distribution of small pore sizes and provide possible starting
505 points for such an analysis. Poiseuille's law would imply that uniform biofilm growth leads
506 to a rescaling of the low-end of the velocity PDF. Figure 3, however, shows that the PDF
507 at low velocities does not follow a simple scaling for growing biofilm. An analysis of the
508 relation of biofilm growth and the evolution of the velocity PDF along these lines is be-
509 yond the scope of this paper and postponed to future work.

510 The results presented here were obtained for four different time points during the
511 early stages of the bioclogging process. Due to the observed exponential evolution of the
512 hydrodynamic quantities in the bioclogged system, the CTRW presented here could be
513 parameterized for any time point within the duration of the experiment (i.e. the bacte-
514 rial exponential growth phase). Exponential growth of biofilms in porous media has been
515 observed previously [*Graf von der Schulenburg et al.*, 2009; *Pintelon et al.*, 2012; *Bottero*
516 *et al.*, 2013; *Hassanpourfard et al.*, 2015], and studied both experimentally and numeri-
517 cally. The work by *Bottero et al.* [2013] and *Hassanpourfard et al.* [2015] found that the
518 exponential growth phase is finite, and that biofilm growth asymptotically approaches a
519 steady state (in terms of biofilm surface coverage or effective porosity, medium permeabil-

ity etc.). *Bottero et al.* [2013] pointed out that steady state biofilm growth is the result of a balance between biomass decay/detachment and growth. The transition from exponential to steady state growth observed by *Bottero et al.* [2013] and *Hassanpourfard et al.* [2015] can be described by a logistic model. In the present study, it was not possible to collect data at long enough temporal scales to observe the transition from exponential growth to steady state.

Interestingly, the propagators obtained in *Seymour et al.* [2004, 2007] exhibited a substantially stronger peak for very small displacements than in the data presented in Figure 5. This could be partially attributed to the Péclet number of our system, which was computed from 3D-PTV data and can be considered to be infinite. Simply, the diffusion experienced by the tracer particles is negligible, meaning that diffusive displacements are not captured in the data presented here. Another aspect lies within differences intrinsic to the experimental approaches used in both studies. Due to the limitations of the 3D-PTV method used in this work, we are only able to sample flow in pores corresponding to the effective porespace and outside the biofilm structure. As a result, completely stagnant or *dead end* pores, which do not participate in flow and are not filled with biomass are not sampled. Similarly, the tracer particles used are too large to penetrate the biomass itself, thus limiting data collected in very low flow regions. In contrast, the MRM method used by *Seymour et al.* [2004] samples flow within the biofilm as well as in all porespaces. This suggests that for low Péclet numbers common in porous media, the permeability of the biofilm itself could affect the transport of solutes [*Dupin et al.*, 2001; *Thullner and Baveye*, 2008; *Ezeuko et al.*, 2011; *Pintelon et al.*, 2012; *Davit et al.*, 2013; *Deng et al.*, 2013]. This has been shown for permeable benthic biofilms, which substantially contributed to transport and reaction processes in gravel bed streams [*Aubeneau et al.*, 2015, 2016; *Li et al.*, 2017].

Finally, we examine how structural changes in the pore geometry due to bioclogging affect the medium permeability. Different relationships between porosity and permeability of the media have been proposed (e.g., *Vandevivere and Baveye* [1992]; *Seki and Miyazaki* [2001]; *Thullner* [2010]). These relationships are either empirical or based on growth models of biofilm in pores (either single pores or simplified pore networks), see *Thullner* [2010] and references therein. The relationships based on growth models can be subdivided into models that assume that biofilms grow homogeneously or in the form of patches. Given that the small pores are clogged first, one might expect to observe a significant change in the flow's heterogeneity, as expressed by the decrease of the shape parameter α , while the permeability is supposedly less affected because highly conductive pores are still open. Changes in permeability would become significant only when the porosity reaches a certain threshold corresponding to clogging of highly conductive zones by biofilm growth. Threshold-based permeability-porosity models along these lines have been proposed in *Bernabé et al.* [2004] for binary mixtures of high- and low-permeability materials and in *Thullner* [2010] for bioclogged media. We note that our measured decrease in the shape parameter α is similar to the relative porosity decrease, while the permeability decreases faster (Table 1). Thus, even though permeability decreases quite sharply, our data are not consistent with threshold-based models, but rather with previously observed trends for permeability decreases in porous media coated with patchy biofilms (e.g., *Graf von der Schulenburg et al.* [2009]; *Thullner* [2010]). Addressing the porosity-permeability relationship more conclusively, however, is beyond the scope of this work.

5 Conclusion

In this work, we successfully monitored the transition from normal to anomalous transport in a progressively bio clogged 3-dimensional porous medium. We observed an exponential evolution of different hydrodynamic quantities consistent with exponential growth kinetics of the biofilm. A two parameter gamma function provided a remarkable description of the bulk and the high tail of the velocity distribution. The shape param-

572 ter α is considered to represent the connectivity of the medium and accounts for a shift
573 from a mainly parallel arrangement of pores towards a more serial one. This too is con-
574 sistent with the observed formation of stagnation zones and preferential flow pathways. A
575 correlated continuous time random walk model that employs stochastic relaxation of ve-
576 locities is able to capture accurately the evolution of the first two spatial moments, but is
577 somewhat limited to reproduce the third moment. Altogether, these insights shed light on
578 the processes behind and provide useful modeling tools to capture the effects of growing
579 biofilm forming bacteria on mass transport processes in porous media. We anticipate that
580 the approach introduced here could also be applied to model transport in other porous me-
581 dia where the heterogeneity is either inherent to the original pore structure or develops
582 dynamically as a consequence of physico-chemical processes.

583 **6 Acknowledgments**

584 We thank Toni Blunschli for manufacturing the flow cells, Peter Desmond for shar-
585 ing the bacteria cultures, Daniel Braun, Lucien Biolley and Ela Burmeister for providing
586 some of the hardware necessary for this study as well as Matthias Willmann for fruitful
587 discussions. Financial support is gratefully acknowledged from the Swiss National Sci-
588 ence Foundation (SNF grant numbers 144645 and 172916) for M.C. and M.H. as well as
589 a SNF mobility grant for doctoral students for M.C.. V.L.M. acknowledges the financial
590 support of the AXA Research fund. M.D. acknowledges the financial support of the Eu-
591 ropean Research Council through the project MHetScale (Grant agreement No. 617511).
592 The particle tracking data is available under the cited reference.

References

- Alim, K., S. Parsa, D. A. Weitz, and M. P. Brenner (2017), Local pore size correlations determine flow distributions in porous media, *Phys. Rev. Lett.*, *119*, 144,501.
- Atekwana, E. A., and E. A. Atekwana (2010), Geophysical signatures of microbial activity at hydrocarbon contaminated sites: A review, *Surveys in Geophysics*, *31*(2), 247–283.
- Aubeneau, A. F., J. D. Drummond, R. Schumer, D. Bolster, J. L. Tank, and A. I. Packman (2015), Effects of benthic and hyporheic reactive transport on breakthrough curves, *Freshwater Science*, *34*(1), 301–315, doi:10.1086/680037.
- Aubeneau, A. F., B. Hanrahan, D. Bolster, and J. Tank (2016), Biofilm growth in gravel bed streams controls solute residence time distributions, *Journal of Geophysical Research: Biogeosciences*, *121*(7), 1840–1850, doi:10.1002/2016JG003333.
- Battin, T. J., W. T. Sloan, S. Kjelleberg, H. Daims, I. M. Head, T. P. Curtis, and L. Eberl (2007), Microbial landscapes: new paths to biofilm research, *Nat Rev Micro*, *5*(1), 76–81.
- Berkowitz, B., H. Scher, and S. E. Silliman (2000), Anomalous transport in laboratory-scale, heterogeneous porous media, *Water Resources Research*, *36*(1), 149–158, doi:10.1029/1999WR900295.
- Bernabé, Y., U. Mok, B. Evans, and F. J. Herrmann (2004), Permeability and storativity of binary mixtures of high- and low-permeability materials, *Journal of Geophysical Research: Solid Earth*, *109*(B12), n/a–n/a, doi:10.1029/2004JB003111, b12207.
- Bianchi, F., M. Thielmann, L. de Arcangelis, and H. J. Herrmann (2018), Critical bursts in filtration, *Phys. Rev. Lett.*, *120*, 034,503, doi:10.1103/PhysRevLett.120.034503.
- Bijeljic, B., A. Raeni, P. Mostaghimi, and M. J. Blunt (2013), Predictions of non-fickian solute transport in different classes of porous media using direct simulation on pore-scale images, *Physical Review E*, *87*(1), 013,011, pRE.
- Bottero, S., T. Storck, T. J. Heimovaara, M. C. M. van Loosdrecht, M. V. Enzien, and C. Picioreanu (2013), Biofilm development and the dynamics of preferential flow paths in porous media, *Biofouling*, *29*(9), 1069–1086, doi:10.1080/08927014.2013.828284.
- Bouwer, E. J., and A. J. B. Zehnder (1993), Bioremediation of organic compounds — putting microbial metabolism to work, *Trends in Biotechnology*, *11*(8), 360–367, doi: [http://dx.doi.org/10.1016/0167-7799\(93\)90159-7](http://dx.doi.org/10.1016/0167-7799(93)90159-7).
- Budwig, R. (1994), Refractive index matching methods for liquid flow investigations, *Experiments in Fluids*, *17*(5), 350–355, doi:10.1007/BF01874416.
- Carrel, M., M. A. Beltran, V. L. Morales, N. Derlon, E. Morgenroth, R. Kaufmann, and M. Holzner (2017), Biofilm imaging in porous media by laboratory x-ray tomography: Combining a non-destructive contrast agent with propagation-based phase-contrast imaging tools, *PLOS ONE*, *12*(7), e0180,374, doi:10.1371/journal.pone.0180374.
- Carrel, M., M. A. Beltran, V. L. Morales, N. Derlon, E. Morgenroth, R. Kaufmann, and M. Holzner (2018a), Bioclogging in porous media - particle trajectory data., *ETH Zurich Research Collection*, doi:10.3929/ethz-b-000237865.
- Carrel, M., V. L. Morales, M. A. Beltran, N. Derlon, R. Kaufmann, E. Morgenroth, and M. Holzner (2018b), Biofilms in 3d porous media: Delineating the influence of the pore network geometry, flow and mass transfer on biofilm development, *Water Research*, *134*, 280 – 291, doi:<https://doi.org/10.1016/j.watres.2018.01.059>.
- Costerton, J. W., P. S. Stewart, and E. P. Greenberg (1999), Bacterial biofilms: A common cause of persistent infections, *Science*, *284*(5418), 1318–1322, doi:10.1126/science.284.5418.1318.
- Coyte, K. Z., H. Tabuteau, E. A. Gaffney, K. R. Foster, and W. M. Durham (2017), Microbial competition in porous environments can select against rapid biofilm growth, *Proceedings of the National Academy of Sciences*, *114*(2), E161–E170, doi:10.1073/pnas.1525228113.
- Cunningham, A. B., W. G. Characklis, F. Abedeen, and D. Crawford (1991), Influence of biofilm accumulation on porous media hydrodynamics, *Environmental science & tech-*

- 646 *nology*, 25(7), 1305–1311.
- 647 Daccord, G., and R. Lenormand (1987), Fractal patterns from chemical dissolution, *Nature*, 325(6099), 41–43, 10.1038/325041a0.
- 648
- 649 Datta, S. S., H. Chiang, T. S. Ramakrishnan, and D. A. Weitz (2013), Spatial fluctuations
650 of fluid velocities in flow through a three-dimensional porous medium, *Physical Review
651 Letters*, 111(6), 064,501, pRL.
- 652 Davit, Y., H. Byrne, J. Osborne, J. Pitt-Francis, D. Gavaghan, and M. Quintard (2013),
653 Hydrodynamic dispersion within porous biofilms, *Physical Review E*, 87(1), 012,718,
654 pRE.
- 655 de Anna, P., T. Le Borgne, M. Dentz, A. M. Tartakovsky, D. Bolster, and P. Davy (2013),
656 Flow intermittency, dispersion, and correlated continuous time random walks in porous
657 media, *Physical Review Letters*, 110(18), 184,502, pRL.
- 658 de Anna, P., B. Quaipe, G. Biros, and R. Juanes (2017), Prediction of the low-velocity dis-
659 tribution from the pore structure in simple porous media, *Phys. Rev. Fluids*, 2, 124,103,
660 doi:10.1103/PhysRevFluids.2.124103.
- 661 Deng, W., M. B. Cardenas, M. F. Kirk, S. J. Altman, and P. C. Bennett (2013), Effect of
662 permeable biofilm on micro- and macro-scale flow and transport in bioclogged pores,
663 *Environmental Science & Technology*, 47(19), 11,092–11,098, doi:10.1021/es402596v.
- 664 Dentz, M., T. Le Borgne, A. Englert, and B. Bijeljic (2011), Mixing, spreading and re-
665 action in heterogeneous media: A brief review, *Journal of Contaminant Hydrology*,
666 120–121, 1–17, doi:http://dx.doi.org/10.1016/j.jconhyd.2010.05.002.
- 667 Dentz, M., P. K. Kang, A. Comolli, T. Le Borgne, and D. R. Lester (2016), Continuous
668 time random walks for the evolution of lagrangian velocities, *Physical Review Fluids*,
669 1(7), 074,004.
- 670 Dentz, M., M. Icardi, and J. J. Hidalgo (2018), Mechanisms of dispersion in a porous
671 medium, *Journal of Fluid Mechanics*, in press.
- 672 Desmond, P., J. P. Best, E. Morgenroth, and N. Derlon (2018), Linking composition of ex-
673 tracellular polymeric substances (eps) to the physical structure and hydraulic resistance
674 of membrane biofilms, *Water Research*, 132, 211 – 221, doi:https://doi.org/10.1016/j.
675 watres.2017.12.058.
- 676 Downie, H., N. Holden, W. Otten, A. J. Spiers, T. A. Valentine, and L. X. Dupuy (2012),
677 Transparent soil for imaging the rhizosphere, *PLoS ONE*, 7(9), e44,276, doi:10.1371/
678 journal.pone.0044276.
- 679 Dupin, H. J., and P. L. McCarty (1999), Mesoscale and microscale observations of bio-
680 logical growth in a silicon pore imaging element, *Environmental science & technology*,
681 33(8), 1230–1236.
- 682 Dupin, H. J., P. K. Kitanidis, and P. L. McCarty (2001), Pore-scale modeling of biological
683 clogging due to aggregate expansion: A material mechanics approach, *Water Resources
684 Research*, 37(12), 2965–2979, doi:10.1029/2001WR000306.
- 685 Durham, W. M., O. Tranzer, A. Leombruni, and R. Stocker (2012), Division by fluid in-
686 cision: Biofilm patch development in porous media, *Physics of Fluids*, 24(9), 091,107,
687 doi:10.1063/1.4747154.
- 688 Ederly, Y., A. Guadagnini, H. Scher, and B. Berkowitz (2014), Origins of anomalous trans-
689 port in heterogeneous media: Structural and dynamic controls, *Water Resources Re-
690 search*, 50(2), 1490–1505, doi:10.1002/2013WR015111.
- 691 Ezeuko, C., A. Sen, A. Grigoryan, and I. Gates (2011), Pore-network modeling of biofilm
692 evolution in porous media, *Biotechnology and Bioengineering*, 108(10), 2413–2423, doi:
693 10.1002/bit.23183.
- 694 Ginn, T. R., B. D. Wood, K. E. Nelson, T. D. Scheibe, E. M. Murphy, and T. P. Clement
695 (2002), Processes in microbial transport in the natural subsurface, *Advances in Water
696 Resources*, 25(8), 1017–1042, doi:http://dx.doi.org/10.1016/S0309-1708(02)00046-5.
- 697 Gouze, P., T. Le Borgne, R. Leprovost, G. Lods, T. Poidras, and P. Pezard (2008), Non-
698 fickian dispersion in porous media: 1. multiscale measurements using single-well in-
699 jection withdrawal tracer tests, *Water Resources Research*, 44(6), n/a–n/a, doi:10.1029/

- 2007WR006278.
- 700
701 Graf von der Schulenburg, D. A., T. R. R. Pintelon, C. Picioreanu, M. C. M. Van Loos-
702 drecht, and M. L. Johns (2009), Three-dimensional simulations of biofilm growth in
703 porous media, *AIChE Journal*, *55*(2), 494–504, doi:10.1002/aic.11674.
- 704 Gujer, W., and M. Bollner (1986), Design of a nitrifying tertiary trickling filter based on
705 theoretical concepts, *Water Research*, *20*(11), 1353–1362.
- 706 Gülan, U., B. Lüthi, M. Holzner, A. Liberzon, A. Tsinober, and W. Kinzelbach (2012),
707 Experimental study of aortic flow in the ascending aorta via particle tracking velocime-
708 try, *Experiments in Fluids*, *53*(5), 1469–1485, doi:10.1007/s00348-012-1371-8.
- 709 Hall-Stoodley, L., J. W. Costerton, and P. Stoodley (2004), Bacterial biofilms: from the
710 natural environment to infectious diseases, *Nat Rev Micro*, *2*(2), 95–108.
- 711 Hassanpourfard, M., Z. Nikakhtari, R. Ghosh, S. Das, T. Thundat, Y. Liu, and A. Kumar
712 (2015), Bacterial floc mediated rapid streamer formation in creeping flows, *Scientific*
713 *Reports*, *5*, 13,070, doi:10.1038/srep13070[https://www.nature.com/articles/srep13070#](https://www.nature.com/articles/srep13070#supplementary-information)
714 [supplementary-information](https://www.nature.com/articles/srep13070#supplementary-information).
- 715 Head, I. M., D. M. Jones, and S. R. Larter (2003), Biological activity in the deep subsur-
716 face and the origin of heavy oil, *Nature*, *426*(6964), 344–352, 10.1038/nature02134.
- 717 Holzner, M., V. L. Morales, M. Willmann, and M. Dentz (2015), Intermittent lagrangian
718 velocities and accelerations in three-dimensional porous medium flow, *Physical Review*
719 *E*, *92*(1), 013,015, pRE.
- 720 Hoyer, K., M. Holzner, B. Lüthi, M. Guala, A. Liberzon, and W. Kinzelbach (2005), 3d
721 scanning particle tracking velocimetry, *Experiments in Fluids*, *39*(5), 923–934, doi:10.
722 1007/s00348-005-0031-7.
- 723 Jiménez-Martínez, J., M. L. Porter, J. D. Hyman, J. W. Carey, and H. S. Viswanathan
724 (2016), Mixing in a three-phase system: Enhanced production of oil-wet reser-
725 voirs by co2 injection, *Geophysical Research Letters*, *43*(1), 196–205, doi:10.1002/
726 2015GL066787.
- 727 Kang, P. K., P. de Anna, J. P. Nunes, B. Bijeljic, M. J. Blunt, and R. Juanes (2014),
728 Pore-scale intermittent velocity structure underpinning anomalous transport through
729 3-d porous media, *Geophysical Research Letters*, *41*(17), 6184–6190, doi:10.1002/
730 2014GL061475.
- 731 Kang, P. K., M. Dentz, T. Le Borgne, S. Lee, and R. Juanes (2017), Anomalous trans-
732 port in disordered fracture networks: Spatial markov model for dispersion with variable
733 injection modes, *Advances in Water Resources*, doi:[https://doi.org/10.1016/j.advwatres.](https://doi.org/10.1016/j.advwatres.2017.03.024)
734 [2017.03.024](https://doi.org/10.1016/j.advwatres.2017.03.024).
- 735 Kazemifar, F., G. Blois, D. C. Kyritsis, and K. T. Christensen (2016), Quantifying the flow
736 dynamics of supercritical co2–water displacement in a 2d porous micromodel using flu-
737 orescent microscopy and microscopic piv, *Advances in Water Resources*, *95*, 352–368,
738 doi:<http://dx.doi.org/10.1016/j.advwatres.2015.05.011>.
- 739 Kim, D.-S., and H. S. Fogler (2000), Biomass evolution in porous media and its effects
740 on permeability under starvation conditions, *Biotechnology and Bioengineering*, *69*(1),
741 47–56, doi:10.1002/(SICI)1097-0290(20000705)69:1<47::AID-BIT6>3.0.CO;2-N.
- 742 Klump, S., Y. Tomonaga, P. Kienzler, W. Kinzelbach, T. Baumann, D. M. Imboden, and
743 R. Kipfer (2007), Field experiments yield new insights into gas exchange and excess
744 air formation in natural porous media, *Geochimica et Cosmochimica Acta*, *71*(6), 1385–
745 1397, doi:<http://dx.doi.org/10.1016/j.gca.2006.12.006>.
- 746 Knecht, K., M. H. Schroth, R. Schulin, and B. Nowack (2011), Development and eval-
747 uation of micro push–pull tests to investigate micro-scale processes in porous media,
748 *Environmental Science & Technology*, *45*(15), 6460–6467, doi:10.1021/es2009727.
- 749 Kone, T., F. Golfier, L. Orgogozo, C. Oltéan, E. Lefèvre, J. C. Block, and M. A. Buès
750 (2014), Impact of biofilm-induced heterogeneities on solute transport in porous media,
751 *Water Resources Research*, *50*(11), 9103–9119, doi:10.1002/2013WR015213.
- 752 Lappan, R. E., and H. S. Fogler (1996), Reduction of porous media permeability from
753 in situ leuconostoc mesenteroides growth and dextran production, *Biotechnology and*

- 754 *Bioengineering*, 50(1), 6–15.
- 755 Lazar, I., I. G. Petrisor, and T. F. Yen (2007), Microbial enhanced oil recovery
756 (meor), *Petroleum Science and Technology*, 25(11), 1353–1366, doi:10.1080/
757 10916460701287714.
- 758 Le Borgne, T., and P. Gouze (2008), Non-fickian dispersion in porous media: 2. model
759 validation from measurements at different scales, *Water Resources Research*, 44(6), n/a–
760 n/a, doi:10.1029/2007WR006279.
- 761 Le Borgne, T., M. Dentz, and J. Carrera (2008), Lagrangian statistical model for transport
762 in highly heterogeneous velocity fields, *Physical Review Letters*, 101(9), 090,601, pRL.
- 763 Le Borgne, T., M. Dentz, P. Davy, D. Bolster, J. Carrera, J.-R. de Dreuzy, and O. Bour
764 (2011a), Persistence of incomplete mixing: A key to anomalous transport, *Physical Re-
765 view E*, 84(1), 015,301, pRE.
- 766 Le Borgne, T., D. Bolster, M. Dentz, P. de Anna, and A. M. Tartakovsky (2011b), Effec-
767 tive pore-scale dispersion upscaling with a correlated continuous time random walk ap-
768 proach, *Water Resour Res*, 47, W12,538.
- 769 Leis, A. P., S. Schlicher, H. Franke, and M. Strathmann (2005), Optically transparent
770 porous medium for nondestructive studies of microbial biofilm architecture and trans-
771 port dynamics, *Applied and environmental microbiology*, 71(8), 4801–4808.
- 772 Leverenz, H. L., G. Tchobanoglous, and J. L. Darby (2009), Clogging in intermittently
773 dosed sand filters used for wastewater treatment, *Water Research*, 43(3), 695–705, doi:
774 <http://dx.doi.org/10.1016/j.watres.2008.10.054>.
- 775 Li, A., A. F. Aubeneau, D. Bolster, J. L. Tank, and A. I. Packman (2017), Covariation in
776 patterns of turbulence-driven hyporheic flow and denitrification enhances reach-scale
777 nitrogen removal, *Water Resources Research*, pp. n/a–n/a, doi:10.1002/2016WR019949.
- 778 Li, L., C. I. Steefel, M. B. Kowalsky, A. Englert, and S. S. Hubbard (2010), Effects of
779 physical and geochemical heterogeneities on mineral transformation and biomass accu-
780 mulation during biostimulation experiments at rifle, colorado, *Journal of contaminant
781 hydrology*, 112(1), 45–63.
- 782 Linga, G., J. Mathiesen, and F. Renard (2017), Self-similar distributions of fluid velocity
783 and stress heterogeneity in a dissolving porous limestone, *Journal of Geophysical Re-
784 search: Solid Earth*, 122(3), 1726–1743, doi:10.1002/2016JB013536.
- 785 Lüthi, B., A. Tsinober, and W. Kinzelbach (2005), Lagrangian measurement of vorticity
786 dynamics in turbulent flow, *Journal of Fluid Mechanics*, 528, 87–118, doi:doi:10.1017/
787 S0022112004003283.
- 788 Maas, H. G., A. Gruen, and D. Papantoniou (1993), Particle tracking velocimetry in three-
789 dimensional flows, *Experiments in Fluids*, 15(2), 133–146, doi:10.1007/BF00190953.
- 790 Malik, N. A., T. Dracos, and D. A. Papantoniou (1993), Particle tracking velocimetry
791 in three-dimensional flows, *Experiments in Fluids*, 15(4-5), 279–294, doi:10.1007/
792 BF00223406.
- 793 Matyka, M., J. Gołembiewski, and Z. Koza (2016), Power-exponential velocity distribu-
794 tions in disordered porous media, *Physical Review E*, 93(1), 013,110, pRE.
- 795 McGuire, K., J. J. McDonnell, M. Weiler, C. Kendall, B. McGlynn, J. Welker, and J. Seib-
796 ert (2005), The role of topography on catchment-scale water residence time, *Water Re-
797 sources Research*, 41(5).
- 798 Menke, H. P., B. Bijeljic, M. G. Andrew, and M. J. Blunt (2015), Dynamic three-
799 dimensional pore-scale imaging of reaction in a carbonate at reservoir conditions, *En-
800 vironmental Science & Technology*, 49(7), 4407–4414, doi:10.1021/es505789f.
- 801 Meyer, D. W., and B. Bijeljic (2016), Pore-scale dispersion: Bridging the gap between
802 microscopic pore structure and the emerging macroscopic transport behavior, *Physical
803 Review E*, 94(1), 013,107, pRE.
- 804 Michalec, F.-G., S. Souissi, and M. Holzner (2015), Turbulence triggers vigorous swim-
805 ming but hinders motion strategy in planktonic copepods, *Journal of The Royal Society
806 Interface*, 12(106).

- 807 Morales, V. L., M. Dentz, M. Willmann, and M. Holzner (2017), Stochastic dynamics
808 of intermittent pore-scale particle motion in three-dimensional porous media: Exper-
809 iments and theory, *Geophysical Research Letters*, 44(18), 9361–9371, doi:10.1002/
810 2017GL074326, 2017GL074326.
- 811 Morgenroth, E., and K. Milferstedt (2009), Biofilm engineering: linking biofilm de-
812 velopment at different length and time scales, *Reviews in Environmental Science and*
813 *Bio/Technology*, 8(3), 203–208.
- 814 Moroni, M., and J. H. Cushman (2001), Statistical mechanics with three-dimensional par-
815 ticle tracking velocimetry experiments in the study of anomalous dispersion. ii. exper-
816 iments, *Physics of Fluids (1994-present)*, 13(1), 81–91, doi:doi:http://dx.doi.org/10.1063/
817 1.1328076.
- 818 Moroni, M., N. Kleinfelder, and J. H. Cushman (2007), Analysis of dispersion in porous
819 media via matched-index particle tracking velocimetry experiments, *Advances in Water*
820 *Resources*, 30(1), 1–15, doi:http://dx.doi.org/10.1016/j.advwatres.2006.02.005.
- 821 Nadell, C. D., D. Ricaurte, J. Yan, K. Drescher, and B. L. Bassler (2017), Flow environ-
822 ment and matrix structure interact to determine spatial competition in pseudomonas
823 aeruginosa biofilms, *eLife*, 6, e21,855, doi:10.7554/eLife.21855.
- 824 Noiriél, C., P. Gouze, and B. Madé (2013), 3d analysis of geometry and flow changes in
825 a limestone fracture during dissolution, *Journal of Hydrology*, 486, 211–223, doi:http:
826 //dx.doi.org/10.1016/j.jhydrol.2013.01.035.
- 827 Pintelon, T. R., C. Picioreanu, M. C. van Loosdrecht, and M. L. Johns (2012), The effect
828 of biofilm permeability on bio-clogging of porous media, *Biotechnology and Bioengi-*
829 *neering*, 109(4), 1031–1042, doi:10.1002/bit.24381.
- 830 Pintelon, T. R. R., D. A. Graf von der Schulenburg, and M. L. Johns (2009), Towards
831 optimum permeability reduction in porous media using biofilm growth simulations,
832 *Biotechnology and Bioengineering*, 103(4), 767–779, doi:10.1002/bit.22303.
- 833 Saffman, P. (1959), A theory of dispersion in a porous medium, *Journal of Fluid Mechan-*
834 *ics*, 6, 321–349.
- 835 Saha, D., M. Soos, B. Lüthi, M. Holzner, A. Liberzon, M. U. Babler, and W. Kinzelbach
836 (2014), Experimental characterization of breakage rate of colloidal aggregates in ax-
837 isymmetric extensional flow, *Langmuir*, 30(48), 14,385–14,395, doi:10.1021/la502686b.
- 838 Sakthivadivel, R., and H. Einstein (1970), Clogging of porous column of spheres by sedi-
839 ment, *Journal of the Hydraulics Division*, 96(2), 461–472.
- 840 Schmidt, L., I. Fouxon, D. Krug, M. van Reeuwijk, and M. Holzner (2016), Clustering of
841 particles in turbulence due to phoresis, *Physical Review E*, 93(6), 063,110, pRE.
- 842 Seki, K., and T. Miyazaki (2001), A mathematical model for biological clogging of
843 uniform porous media, *Water Resources Research*, 37(12), 2995–2999, doi:10.1029/
844 2001WR000395.
- 845 Seki, K., M. Thullner, J. Hanada, and T. Miyazaki (2006), Moderate bioclogging lead-
846 ing to preferential flow paths in biobarriers, *Ground Water Monitoring & Remediation*,
847 26(3), 68–76, doi:10.1111/j.1745-6592.2006.00086.x.
- 848 Seymour, J. D., J. P. Gage, S. L. Codd, and R. Gerlach (2004), Anomalous fluid transport
849 in porous media induced by biofilm growth, *Physical Review Letters*, 93(19), 198,103,
850 pRL.
- 851 Seymour, J. D., J. P. Gage, S. L. Codd, and R. Gerlach (2007), Magnetic resonance mi-
852 croscopy of biofouling induced scale dependent transport in porous media, *Advances in*
853 *Water Resources*, 30(6–7), 1408–1420, doi:http://dx.doi.org/10.1016/j.advwatres.2006.05.
854 029.
- 855 Shen, J., and R. Ni (2017), Experimental investigation of clogging dynamics in homo-
856 geneous porous medium, *Water Resources Research*, 53(3), 1879–1890, doi:10.1002/
857 2016WR019421.
- 858 Siena, M., M. Riva, J. D. Hyman, C. L. Winter, and A. Guadagnini (2014), Relation-
859 ship between pore size and velocity probability distributions in stochastically generated
860 porous media, *Physical Review E*, 89(1), 013,018, pRE.

- 861 Stoodley, P., D. deBeer, and Z. Lewandowski (1994), Liquid flow in biofilm systems, *Ap-*
862 *plied and Environmental Microbiology*, 60, 2711–2716.
- 863 Taylor, S. W., and P. R. Jaffé (1990), Biofilm growth and the related changes in the phys-
864 ical properties of a porous medium: 3. dispersivity and model verification, *Water re-*
865 *sources research*, 26(9), 2171–2180.
- 866 Thullner, M. (2010), Comparison of bioclogging effects in saturated porous media within
867 one- and two-dimensional flow systems, *Ecological Engineering*, 36(2), 176 – 196, doi:
868 <https://doi.org/10.1016/j.ecoleng.2008.12.037>, special Issue: BioGeoCivil Engineering.
- 869 Thullner, M., and P. Baveye (2008), Computational pore network modeling of the influ-
870 ence of biofilm permeability on bioclogging in porous media, *Biotechnology and Bio-*
871 *engineering*, 99(6), 1337–1351, doi:10.1002/bit.21708.
- 872 Thullner, M., L. Mauclaire, M. H. Schroth, W. Kinzelbach, and J. Zeyer (2002), In-
873 teraction between water flow and spatial distribution of microbial growth in a two-
874 dimensional flow field in saturated porous media, *Journal of contaminant hydrology*,
875 58(3), 169–189.
- 876 Vandevivere, P., and P. Baveye (1992), Saturated hydraulic conductivity reduction caused
877 by aerobic bacteria in sand columns, *Soil Science Society of America Journal*, 56(1), 1–
878 13.
- 879 Wen, H., and L. Li (2017), An upscaled rate law for magnesite dissolution in heteroge-
880 neous porous media, *Geochimica et Cosmochimica Acta*, 210, 289–305.
- 881 Xu, H. (2008), Tracking lagrangian trajectories in position–velocity space, *Measurement*
882 *Science and Technology*, 19(7), 075,105.
- 883 Yao, K.-M., M. T. Habibian, and C. R. O’Melia (1971), Water and waste water filtration.
884 concepts and applications, *Environmental science and technology*, 5(11), 1105–1112.